Self-Assembly of $SbCl_3$ and 1,4-Dioxane: Cubic Structure Connected by Very Weak Bonds

Jeremy Kua,*,† Rowena C. Daly,† Keaton M. Tomlin,† Adri C. T. van Duin,‡ Thomas B. Brill,§ Royce W. Beal,# and Arnold L. Rheingold¶

Department of Chemistry and Biochemistry, University of San Diego, 5998 Alcala Park, San Diego, California 92110, Department of Mechanical and Nuclear Engineering, Pennsylvania State University, 136 Research East Building, Bigler Road, University Park, Pennsylvania 16802, Department of Chemistry, University of Delaware, 102 Brown Laboratory, Newark, Delaware 19716, Hill Air Force Base, Ogden, Utah 84054, and Department of Chemistry and Biochemistry, University of California San Diego, 9500 Gilman Drive, La Jolla, California 92093

Received: August 25, 2009

The self-assembly of $SbCl_3$ and 1,4-dioxane in a 2:3 ratio leads to an interpenetrating extended cubic structure from X-ray crystallography. The structure is held together by very weak Sb−O bonds (∼7 kcal/mol each), which still maintain strong directionality. Parameterization and subsequent simulation of the system using a reactive force field (ReaxFF) gives us insight into the key interactions necessary for self-assembly from a completely random configuration of molecules into the experimentally observed cubic structure. We explain why the porous structure (with no interpenetration of lattices) is not observed, and we trace the important intermediate substructures formed en route to the crystal.

Introduction

Self-assembly is a key feature in building complex structures from simpler components. This process is ubiquitous in nature, be it the formation of crystals, amorphous substances, or the myriad macromolecules of life. Synthetic self-assembled structures have come a long way in both complexity and potential applications, particularly in the development of new materials. Some very recent reviews covering modeling, synthesis, and applications of materials include nonbonded interactions in soft materials,[1] bioinorganic nanohybrids,[2] polymers on surfaces,[3] gas storage in nanoporous materials,[4] boronic acid molecular self-assembly,[5] and challenges in nanometer scale fabrication.[6]

Antimony and bismuth trihalides are known to form octahedral complexes with nucleophilic ligands.[7−9] Three nucleophilic centers form weak covalent bonds with each antimony or bismuth center. Complexes that have been synthesized have used ligands such as tetrahydrofuran,[10] *N*,*N*′-bidentate ligands,[11] phosphines/arsines,[12] and seleno-ethers.[13,14] Several of these reported complexes are polymeric, observed when using bidentate and tridentate ligands. There is also a published synthesis and cubic crystal structure of the 2:3 $SbCl_3$ and 1,4-dioxane adduct;[15] the structure, however is highly problematic as described in Supporting Information.

Our goal is to study the dynamics of self-assembly of the cubic structure formed in a 2:3 ratio of $SbCl_3$ and 1,4-dioxane via molecular dynamics simulations. If each $SbCl_3$ forms 3 Sb−O bonds (to three dioxane molecules) at approximately 90° bond angles to each other, 8 $SbCl_3$ molecules could form the corners of a cube with 12 bridging dioxane molecules creating a nanopore as shown in Figure 1. In addition, the Sb−O bonds are weak (∼7 kcal/mol apiece), and the structure is expected to be dynamic rather than static and rigid. Several nanoporous materials that can dynamically adjust to the presence and absence of guest molecules have been recently synthesized based on metal−organic framework architecture.[16−19] This nanoporous "perfect" cube turns out to be unstable as observed both from our simulations and from our X-ray crystallographic analysis.

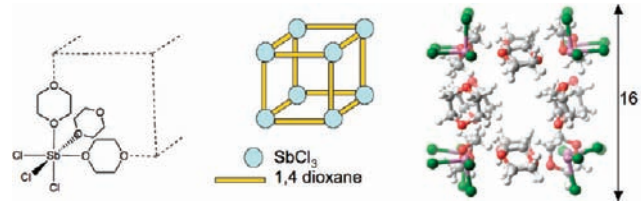

Figure 1. Hypothetical "perfect" cube formed by 8 $SbCl_3$ and 12 dioxane molecules.

We have obtained high-quality crystal structures of the 2:3 $SbCl_3$/1,4-dioxane system (which is the central focus of this study) along with the structures of the isomorphous dioxanates of $AsCl_3$, $AsBr_3$, and $SbBr_3$. Although the crystal structure has cubic symmetry, the nanoporous perfect cube shown in Figure 1 is not found. Instead, an interpenetrating structure with 16 $SbCl_3$ and 24 dioxane molecules per unit cell, double the number expected in the simple cube, is formed as shown in Figure 2. The easiest way to visualize this structure is to imagine $SbCl_3$ molecules placed on a 4 × 4 × 4 grid at positions at the (0,0), (0,2), (2,0), and (2,2) positions in Layers 1 and 3 and at (1,1), (1,3), (3,1), and (3,3) positions in Layers 2 and 4. A schematic of this structure is shown in Figure 2, shown as a 5 × 5 grid since repeating the edges makes the overall pattern easier to visualize. The dioxane molecules are drawn slightly displaced from the grid lines and points for visual purposes so that all of the grid lines are visible. The tiny squares adjoining several grid points are dioxane molecules crossing layers bridging $SbCl_3$ molecules above and below the plane. Crystallographic data is described in Methods. A telescopic view of the crystal is shown in Figure 3.

* Corresponding author. E-mail: jkua@sandiego.edu.
† University of San Diego.
‡ Pennsylvania State University.
§ University of Delaware.
# Hill Air Force Base.
¶ University of California San Diego.

10.1021/jp908205x CCC: $40.75
Published on Web 09/28/2009

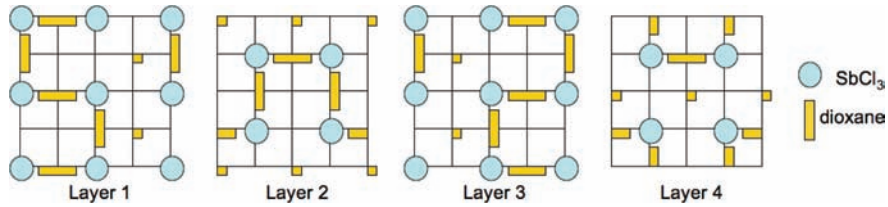

Figure 2. Schematic of the 16 $SbCl_3$ and 24 dioxane interpenetrating crystal lattice unit cell.

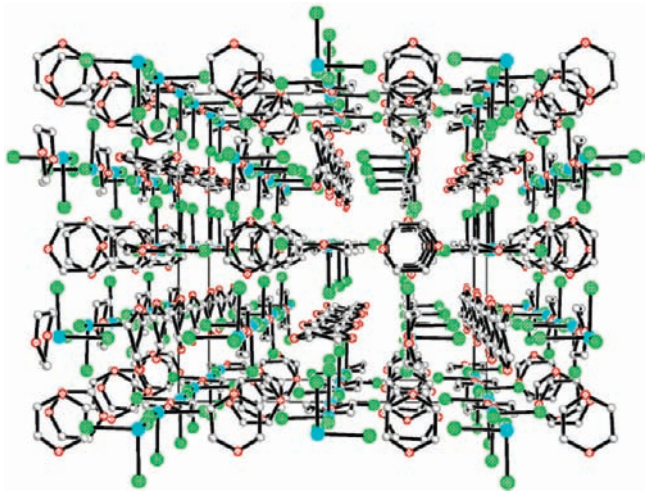

Figure 3. Telescopic view of the 2:3 $SbCl_3$ and dioxane adduct crystal structure (Sb = blue, Cl = green, O = red, C = gray).

To study the dynamics of self-assembly of $SbCl_3$ and dioxane, we will need to simulate a system containing hundreds of atoms involved in making and breaking bonds in the nanosecond (ns) time scale. Ab initio quantum mechanics (QM) methods would take too long for this period, while conventional force fields using standard molecular dynamics (MD) techniques cannot simulate directional covalent bonds breaking and forming. The ReaxFF reactive force field has been developed to bridge this gap. Originally parametrized for hydrocarbons,[20] ReaxFF has been extended to study a variety of systems including high energy materials,[21] metal-catalyzed carbon nanotube formation,[22] metal hydrides,[23] and catalysis on metals[24] and metal oxides.[25] In the present study, we have parametrized the force field for $SbCl_3$ and interaction terms for $SbCl_3$ to organic systems containing C, H, O atoms. Subsequently, we ran a series of ReaxFF simulations under different starting conditions to elucidate the self-assembly process.

We find that $SbCl_3$ and 1,4-dioxane prefer to form the interpenetrating crystal structure rather than the perfect cube to reduce void space. However, we find that on average only 61% of these interactions remain intact at 300 K at a density similar to the crystal. We have also traced the evolution of completely disordered random starting structures of $SbCl_3$ and dioxane to identify the important substructures en route to assembling the crystal.

Methods

Experimental Synthesis. $AsCl_3$, $AsBr_3$, $SbCl_3$, and $SbBr_3$ were obtained from Sigma-Aldrich and used as obtained. All of the complexes were made in the same way. In a glovebox, to approximately 5 mL of 1,4-dioxane (Aldrich anhydrous stored over molecular sieve) in a vial was added approximately 1 g of the Gp-15 trihalide. In the case of $AsCl_3$, which is a liquid at room temperature, a white precipitate was formed with no discernible delay. The other three became slowly turbid and ultimately formed a precipitate over a period of about 2 min. In the solution above, both of the bromide precipitates became light yellow. A sample of the precipitate was collected, dried on filter paper, and placed in a separate vial. The vials were then placed in a vacuum for several minutes and then backfilled with N_2. These vials were flame-sealed and left to stand. In the case of the arsenic compounds, useful single crystals began to grow by sublimation on the sides of the vials within a few days. In the case of the less volatile antimony compounds, the vials were placed on a warmed surface at about 35 °C for several weeks. All compounds had melting points in good agreement with the literature.[9]

TABLE 1: Crystallographic Data for $SbCl_3$/1,4-Dioxane

	$2SbCl_3$•3dioxane
empirical formula	$C_6H_{12}SbCl_3O_3$
formula weight	360.26
space group	Cubic, *I*-43*d*
a, Å	16.92961 (10)
volume, Å^3	4852.22 (5)
Z	16
D(calcd), gcm^{-3}	1.973
rflns collected, unique	6753, 712
completeness (%), *R*(int)	99.7, 0.0433
*R*1, *wR*2 ($I > 2\sigma$)	0.0265, 0.0573
*R*1, *wR*2 (all data)	0.0309, 0.0602
GOF on F^2	1.144

TABLE 2: Experimental Bond Lengths and Angles of $SbCl_3$/1,4-Dioxane

	$2SbCl_3$•3dioxane
E-X, Å	2.3763 (9)
E-X, Å (pure EX_3)	2.359 (5)[a]
E-O, Å	2.760 (1)
X-E-X, deg	92.97 (6)
X-E-X, deg (pure EX_3)	93.39 (5)[a]

[a] Lipka, A. *Acta Crystallogr.* **1979**, *B35*, 3020.

X-ray Crystallography. Crystallographic data of 2:3 $SbCl_3$/1,4-dioxane is summarized in Table 1, and experimental bond lengths and angles are found in Table 2. All data were obtained at 173 K with a Siemens P4 diffractometer equipped with an APEX CCD detector. (Data for the isomorphous dioxanates of $AsCl_3$, $AsBr_3$, and $SbBr_3$ are provided in Supporting Information.) The cubic space group *I*-43*d* was uniquely determined by systematic absences in the diffraction data. The $SbCl_3$/1,4-dioxane complex was solved by direct methods. All non-hydrogen atoms were anisotropically refined. All dioxane molecules are inherently disordered about their 2-fold site symmetry, and hydrogen atoms were placed in idealized locations. All data collection and refinement software is contained in the libraries maintained by Bruker-AXS, Madison, WI.

Quantum Mechanical Calculations. All calculations were carried out using Jaguar 6.0[26] at the B3LYP[27−30] level of density functional theory (DFT). This functional was chosen to be consistent with parametrizations of other elements in ReaxFF.

TABLE 3: Comparison of ReaxFF, QM, and Experimental Data for $SbCl_3$

	ReaxFF	QM	experimental
Sb−Cl bond distance (Å)	2.40	2.41	2.36
Cl−Sb−Cl angle (°)	100	99	95
Sb charge (a.u.)	+0.58	+0.67	
Cl charge (a.u.)	−0.19	−0.22	

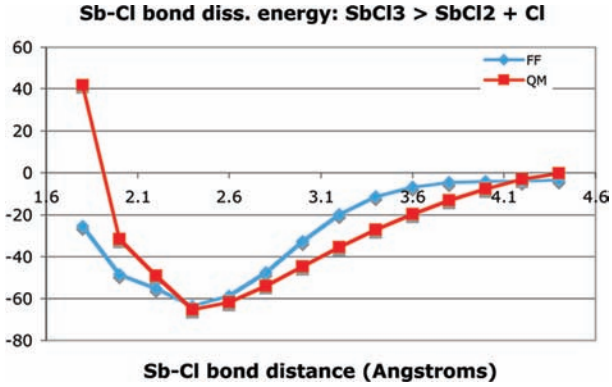

Figure 4. QM and ReaxFF bond dissociation curve for the Sb−Cl bond in $SbCl_3$.

For Sb, the Hay and Wadt core−valence relativistic effective core potential (ECP)[31] denoted LACVP in the Jaguar program was used. This is a nonlocal ECP using angular momentum projection operators to enforce the Pauli principle. All other atoms were treated with the 6-31G**++ basis set. Electrostatic potential (ESP) fitted charges were calculated and used to parametrize the force field. Zero point energies and enthalpy corrections were not included, again to be consistent with previous parametrizations that used only the electronic energies. Full geometry optimizations were performed for all structures. To calculate the potential energy curve along a chosen reaction coordinate, only the reaction coordinate was constrained at fixed distances (or angles) and the rest of the molecule was optimized at each step. Since the Sb−O bond between $SbCl_3$ and 1,4-dioxane is weak, we double-checked our calculated structures and binding energy at the MP2 level and found good agreement with B3LYP values (see Supporting Information).

Parameterization of the Reactive Force Field. No further parametrization of dioxane was performed; we used the existing parameters that were successful in simulating hydrocarbon oxidation, which contained the necessary C, H, O parameters.[32] However, we did include dimethylether (DME) in the training set to ensure that the Sb−O bond was properly described. Details of ReaxFF parametrization have already been described extensively;[20−25,32] therefore, we will just describe details of only key interactions. The full training set and force field parameters can be found in Supporting Information.

For $SbCl_3$, ReaxFF reproduces the QM calculations well for bond distances and angles, both of which are reasonably close to experimental values from the $SbCl_3$ crystal structure.[33] There is a 0.1 au charge difference between ReaxFF and QM for Sb; the difference for Cl is 0.03 au. These geometry and charge comparisons are listed in Table 3. For the Sb−Cl bond dissociation curve of $SbCl_3$ shown in Figure 4, we see that ReaxFF does a good job reproducing the optimum distance and total bond dissociation energy from QM, but the shape of the curve is not as well reproduced particularly at the repulsive end. However, since the Sb−Cl bond is sufficiently strong and not expected to undergo dissociation at simulations near room temperature, this was not a source of concern for our simulations. The Cl−Sb−Cl angle bend was well reproduced by ReaxFF (see Figure 5). Throughout our simulations, no bizarre or unphysical behavior was observed in the $SbCl_3$ molecules, and the bond distances and angles stayed close to experimental values.

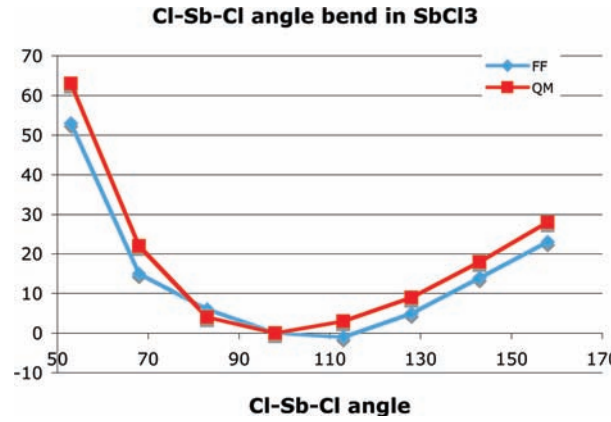

Figure 5. QM and ReaxFF angle distortion curve for the Cl−Sb−Cl angle in $SbCl_3$.

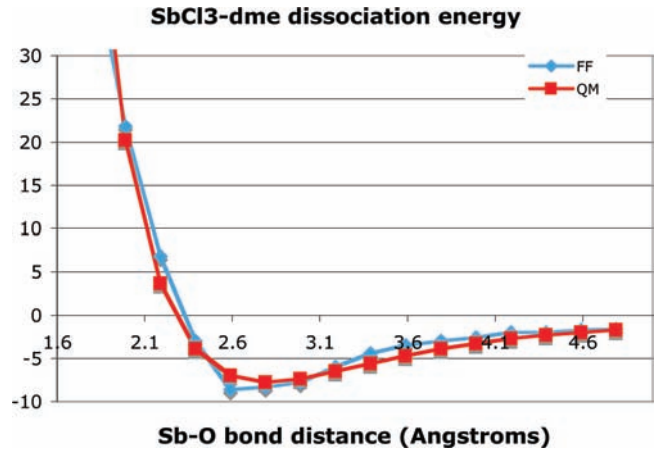

Figure 6. QM and ReaxFF bond dissociation curve for the Sb−O bond in $SbCl_3$•DME.

TABLE 4: Reaction Energies for Binding of DME to $SbCl_3$

	ReaxFF (kcal/mol)	QM (kcal/mol)
$SbCl_3$ + DME → $SbCl_3$•DME	−8.6	−7.8
$SbCl_3$ + 2 DME → $SbCl_3$•2DME	−14.5	−15.6
$SbCl_3$ + 3 DME → $SbCl_3$•3DME	−22.4	−21.7

The most important interaction to consider is the bond dissociation curve for the Sb−O bond. As shown in Figure 6, ReaxFF does an excellent job reproducing the shape of the QM curve for the Sb−O bond in $SbCl_3$•DME. The force field shortens the bond marginally compared with QM but does an excellent job reproducing the bond dissociation energy. We did not fit the dissociation curves for the larger systems $SbCl_3$•2DME and $SbCl_3$•3DME, but once again the total bond dissociation energies are well reproduced as shown in Table 4.

Molecular Dynamics Simulations. All NVT MD simulations were performed under periodic boundary conditions, using the velocity Verlet algorithm and a time step of 0.25 fs. Smaller time steps are required for ReaxFF compared with conventional force field simulations because the charges and bond orders are allowed to change every time step. The system temperature was controlled by a Berendsen thermostat with a temperature-damping constant of 100 fs.[34] We studied several systems

containing either 8 $SbCl_3$/12 dioxane or 16 $SbCl_3$/24 dioxane, considering both highly structured and random starting configurations, at different temperatures and densities. The varying setup for each system is described in Results and Discussion. The simulations are typically run in 100 ps blocks with geometry snapshots written every 100 steps (25 fs). Thus for a 100 ps block, our analyses are based on 4000 structures. On several occasions where changes are taking place quickly, we have analyzed 10 ps blocks for a total of 400 structures.

Results and Discussion

8 $SbCl_3$/12 Dioxane Cube. The 8 $SbCl_3$/12 dioxane cube shown in Figure 1 was built using the Spartan program.[35] We chose a simulation cell size of 16 × 16 × 16 Å^3 to keep the corner $SbCl_3$ molecules of separate cubes at approximately van der Waals distances to each other. In the perfect cube, there are 24 Sb−O bonds. For analysis purposes, we define an Sb−O interaction as being a bond for distances less than 3 Å. The overall percentage of Sb−O bonds formed over the course of the simulation is calculated by counting the number of Sb−O bonds present in each snapshot and comparing that number to the perfect cube. Throughout the text we will designate this value %SbO. Because bonds are constantly being broken and reformed, this percentage does not necessarily correspond to the absolute number of Sb−O bonds present. Some of the Sb−O bonds will stay intact over the course of a simulation window, others will fluctuate being present part of the time, and some will be mostly absent or broken most of the time. When referring to the absolute number of Sb−O bonds present, we will typically classify them as "*x* out of 24 bonds" intact (present most of the time) or partial/labile (present part of the time).

In the first 100 ps window at 10 K, some of the Sb−O bonds are broken, and we observe dioxane molecules moving to occupy the void space in the center of the cube. The %SbO in this 100 ps window averages 85%. Near the 100 ps mark, 16 out of 24 bonds remain intact, while 3 out of 24 are partial. In the next window (100−200 ps), %SbO drops to 67% with 16 out of 24 bonds remaining intact. These values hold steady with longer simulation times.

If heated to 100 K, %SbO drops to 55% within the first 100 ps and remains constant (no change up to 500 ps); 13 out of 24 bonds remain intact. At 200 K, %SbO drops to 46% and then holds steady with 11 out of 24 bonds intact. The structure is relatively disordered, and in fact, we will see that starting from a random configuration (as discussed in the next section) will lead to a similar %SbO. At 300 K, %SbO drops rapidly to 29% in the first 100 ps but then increases back up to 38% within the next window (100−200 ps) and holds steady with longer simulation times; this equilibrated value also corresponds closely to what we will observe starting from a random configuration. At this point, only 7 out of 24 bonds remain intact while 5 out of 24 are partially present 20−70% of the time. Hence, we surmise that our calculations are relatively well-converged, and we conclude that the perfect cube shown in Figure 1 is unstable. The bonds are too weak to support a structure with so much void space.

8 $SbCl_3$/12 Dioxane Random Starting Configuration. To generate random starting configurations that do not initially have bad van der Waals overlap, we randomly placed the molecules in a 20 × 20 × 20 Å^3 simulation cell, minimized the structure, then ran molecular dynamics while compressing the cell lengths at a rate of 0.4 Å per picosecond until the desired size is reached. We first examined simulation cells of 16 × 16 × 16 Å^3 to compare with the perfect cube simulations described above.

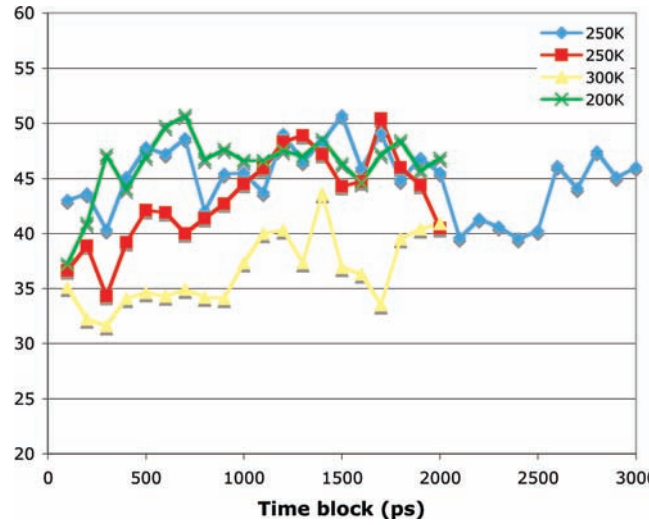

Figure 7. Percentage of Sb−O bonds formed starting from random configurations of 8 $SbCl_3$ and 12 dioxane in a 16 × 16 × 16 Å^3 simulation cell with different temperature runs.

Figure 7 shows how %SbO values vary at different temperatures. Each point on the graph represents the %SbO for a 100 ps block (4000 snapshots). Two of the runs with different random starting configurations are at the same temperature (250 K) so the reader has a sense of the fluctuations observed. If we average all of the points for each temperature, we find that %SbO increases as temperature decreases; at 300, 250, and 200 K, the averages are 37, 44, and 46% respectively. After the first 500 ps, the fluctuation in %SbO is approximately 10% at 250 and 300 K, and approximately 5% at 200 K. The converged values of 37 and 46% at 200 and 300 K correspond very closely with what we find when the perfect cube breaks down at these same temperatures, as described in the previous section. This further supports our conclusion that the perfect cube is unstable and breaks down into a relatively disordered structure.

The density of 8 $SbCl_3$/12 dioxane in a 16 × 16 × 16 Å^3 box is 1.17 g/cm^3. We know from our simulations of the perfect cube that there is too much void space for the structure to be stable. In fact, the experimental density from the crystal structure is 1.95 g/cm^3. Hence, we examined how Sb−O interactions would change as a function of density. This is shown in Figure 8 where all simulations are run at 300 K. The legend in the figure corresponds to the cube length in Å. The %SbO values at different densities are listed in Table 5. We find that, in general, %SbO increases with density. At the experimental density of 1.95 g/cm^3, this value is 45%. Interestingly, at 2.18 g/cm^3, the percentage shoots up in the 300−600 ps window and then plateaus at around 62%. However, compressing the cell further to 2.77 g/cm^3 did not increase %SbO; in fact, this value plateaus at a slightly lower percentage. Since we are interested in studying the system that corresponds most closely to experiment, we did not pursue these simulations further and instead concentrated on analyzing the 1.95 g/cm^3 system corresponding to a simulation cell size of 13.5 × 13.5 × 13.5 Å^3.

The data we have presented up to this point have been more global in scope; the percentage of Sb−O bonds present is averaged over thousands of structures. To analyze individual interactions, we can focus on one $SbCl_3$, monitor how it interacts with its three closest dioxanes, and thus gauge how dynamic the Sb−O bonds are throughout the simulation. From a 2 ns simulation at 300 K, Figure 9 shows that the first bond (Sb1−O9) is formed at the beginning of the simulation and stays

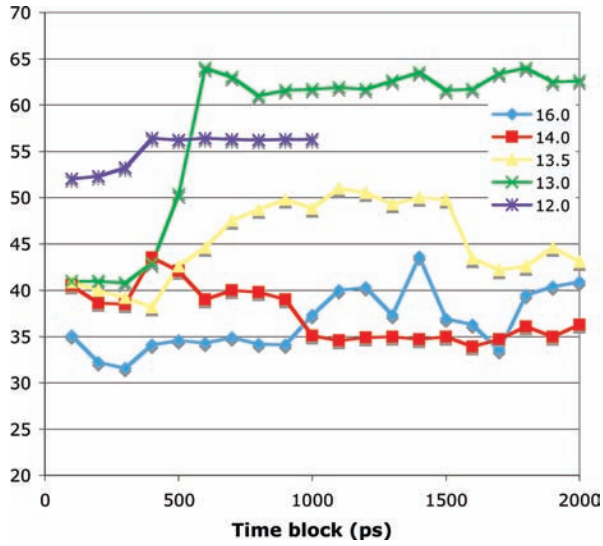

Figure 8. Percentage of Sb−O bonds formed starting from random configurations of 8 $SbCl_3$ and 12 dioxane at 300 K with different simulation cell size runs.

TABLE 5: Average Percentage of Sb−O Bonds Formed Starting from Random Configurations of 8 $SbCl_3$ and 12 Dioxane at 300 K at Different Densities

simulation cell size (Å^3)	density (g/cm^3)	% Sb−O bonds formed
16 × 16 × 16	1.17	36.6%
14 × 14 × 14	1.74	37.3%
13.5 × 13.5 × 13.5	1.95	45.3%
13 × 13 × 13	2.18	57.6%
12 × 12 × 12	2.77	55.2%

stable throughout the length of the simulation. The second bond (Sb1−O4) forms shortly after 600 ps. It breaks many times throughout the course of the simulation where the bond distance increases to approximately 5 Å momentarily and quickly reforms. The third bond (Sb1−O2) only starts to become stable after 1 ns and remains more labile than the other two.

The $SbCl_3$ that we focused on in our analysis is rather unique in that none of the other $SbCl_3$ molecules form three Sb−O bonds with dioxane; rather, one or two bonds is typical. Figure 10 shows the percentage of bonds formed in the first 1 ns split into 10 blocks of 100 ps each. Interactions formed for less than 10% of each simulation window are not included. We see that a chain starts to form involving Sb1, Sb7, and Sb6. The bond between Sb1 and dioxane 4 starts to form in the latter part of this period. Sb4 is isolated with a single dioxane. Sb2 switches from interacting with dioxane 10 in the first half of the period to dioxane 11 in the second half. Accompanying this change is the other end of the dioxane 11 switching between Sb5 and Sb8.

In the next 1 ns window, shown in Figure 11, there is now one long chain connecting six of the eight $SbCl_3$ molecules although the bridges formed by dioxanes 3 and 11 are more tenuous. Dioxane 3 is labile, constantly breaking and reforming its bonds to both Sb6 (as shown by the Sb6−O3 row with percentages ranging from 15 to 68%) and Sb3 (as shown by the Sb3−O3 row with percentages ranging from 24 to 63%). Dioxane 11 on the other hand forms a stable bond with Sb8 for the first half of the window, but there is no bond throughout the second half (Sb8−O11 row). We conclude from the 8 $SbCl_3$/12 dioxane simulations that the perfect cube is not formed because it is unstable. Chains are formed whereby each $SbCl_3$ forms good interactions with one or two dioxane molecules but rarely more. The structure is relatively disordered.

16 $SbCl_3$/24 Dioxane Crystal. The 16 $SbCl_3$/24 dioxane interpenetrating structure shown in Figure 2 was generated from the crystal structure coordinates. The crystal has a cell size of 17 × 17 × 17 Å^3 corresponding to the experimental density of 1.95 g/cm^3. In this ideal structure, there are 48 Sb−O bonds. As with the smaller system, we define an Sb−O interaction as being a bond for distances less than 3 Å. Similarly, %SbO is calculated by counting the number of Sb−O bonds present in each snapshot, averaged over the course of a simulation window.

If the simulation is run at 10 K, the crystal structure stays intact. However, at 250 or 300 K, we begin to observe a number of Sb−O bonds breaking. We infer that, because the bonds are quite weak (~7 kcal/mol each), entropic considerations lead to a less ordered average structure in solution. The value of %SbO drops and plateaus at 61% for simulations at both 250 and 300 K, as shown in Figure 12. This plateau is reached after 1.5 ns for the 300 K simulation and 3 ns for the 250 K simulation. The first point in the figure is not at 100% because there was a 100 ps equilibration period whereby the structure was slowly heated in 10 K increments every 2.5 ps and then maintained at constant temperature once the desired temperature was reached. There is an average 10% decrease in %SbO during this equilibration.

To examine what is taking place as the crystal experiences disorder, we analyzed the structures in the equilibration period and later simulation windows for the 250 K simulation. (The 300 K simulation shows similar behavior, but we have more data and a longer simulation time at 250 K.) For the first 50 ps of the 100 ps equilibration, although %SbO begins to drop slowly, all 48 Sb−O bonds remain intact and are present more than 90% of the time. During this time, the crystal is still being heated. In the 50−60 ps window, we see three Sb−O bonds fluctuating significantly. In the top panel of Figure 13, one of the Sb−O bonds (in Layer 1) is present 46% of the time, and two others (in Layer 4) are present 61−62% of the time. Sb−O bonds that are intact more than 66% of the simulation window are not labeled; bonds present 34−66% are marked in green; bonds present 5−33% are marked in red, and essentially broken bonds (<5%) are labeled with a black X. In the next 10 ps (middle panel of Figure 13), the structure has reached the target temperature of 250 K. We see that these three Sb−O interactions have weakened further, and they have additionally induced the weakening of other Sb−O interactions in the same plane. A little later (bottom panel of Figure 13), another Sb−O interaction in Layer 1 drops to 52% accompanied by an interaction in the same (cross-section) plane in Layer 3 that drops to 4%. It is important to note that no new Sb−O bonds are being formed during the simulation.

As the simulation is run further, we see that Sb−O bonds are dynamically forming and breaking but that, on average, the crystal structure maintains its integrity (see further discussion and figures in Supporting Information). If we define intact bonds as present at least 67% of the simulation window, then over 3 ns of simulation data, the average number of intact bonds is 31 out of 48. This means that 17 out of 48 bonds are labile in the crystal structure at 250 K.

If this structure is cooled to 100 K, %SbO starts to climb back up to ~68% after 1 ns of dynamics. We also tried cooling the crystal back to 10 K, but the dynamics were too slow to observe large-scale changes. At first glance, it seems incongruous that cooling the crystal does not result in the perfectly ordered crystal; one might postulate that simply running the

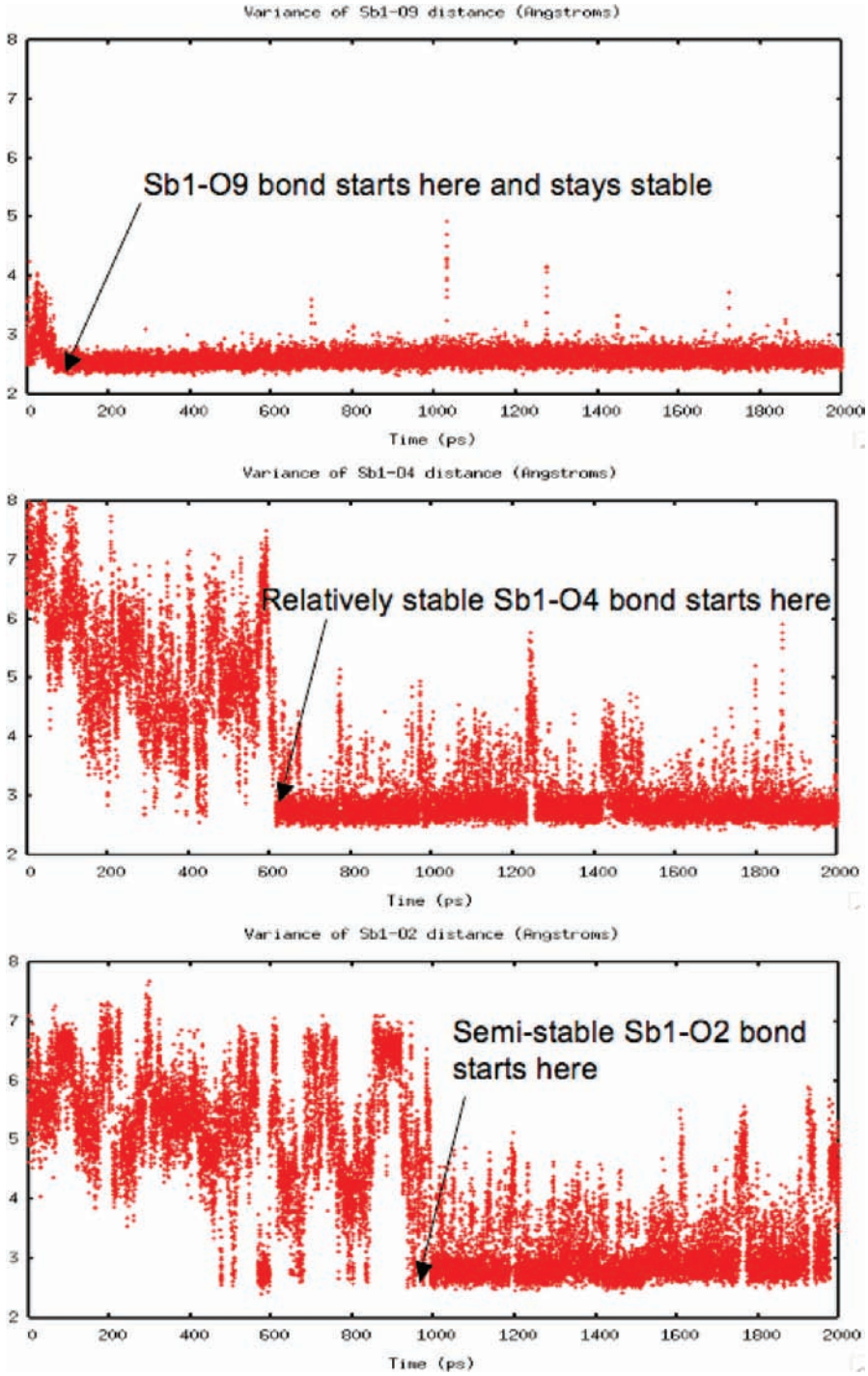

Figure 9. Variance of Sb−O distances of one $SbCl_3$ molecule over 2 ns. An Sb−O bond is defined as being less than 3 Å.

simulation longer (and maybe cooling at a slower rate) will lead to the perfect crystal. We do not think this will be the case in this system because the Sb−O bond is rather weak (7 kcal/mol). The intermolecular attractions in a "liquid" of $SbCl_3$ and dioxane may be substantial, and therefore a small amount of thermal energy is sufficient to lead to the disorder of individual Sb−O bonds in the crystal. The same phenomena is also observed for water; although much more heavily parametrized, predictions of different ice phases with the correct hydrogen-bond networks is still not reproducible from molecular simulations.[36]

To get a rough estimate of the strength of the intermolecular forces, we calculated the solvation energy of individual $SbCl_3$ and dioxane molecules by embedding each in a Poisson−Boltzmann polarizable continuum with dielectric constants representing a range of values that may correspond to the $SbCl_3$/dioxane "solvent". We used three dielectric constants: 2.2 for $SbCl_3$, 12.8 for dioxane, and 7.5 for an average value. Based on the solvation energies in Table 6, we see that the estimated intermolecular forces are probably in the ~6 kcal/mol range, almost as strong as an individual Sb−O bond. Therefore at room temperature, it is not surprising that the average thermal energy in the system results in an entropically driven average structure with %SbO values much lower than 100% and at least one-third of the bonds being labile. The shallow potential energy well for the Sb−O bond (Figure 6) also suggests that a smaller but still significant interaction energy is present even when the bond is lengthened past 3.0 Å.

	1	2	3	4	5	6	7	8	9	10
Sb1-O2						27.8				15.6
Sb1-O4							68.1	86.1	86.6	6.3
Sb1-O9	77.1	100.	99.9	100.	100.	99.9	99.5	99.9	99.7	99.8
Sb1-O10	62.3									
Sb2-O2							19.0		12.8	
Sb2-O10	100.	100.	99.9	100.	99.9	93.7				
Sb2-O11						27.0	99.3	99.5	99.9	100.
Sb3-O1	66.4	100.	100.	92.7	99.1	98.0	100.	100.	100.	100.
Sb3-O2	14.8									
Sb3-O3						15.3				11.0
Sb4-O6	13.6									
Sb4-O7	99.6	100.	100.	99.9	99.9	89.4	99.7	100.	100.	100.
Sb4-O12	16.8				27.0	73.4				
Sb5-O2								20.5	48.3	20.7
Sb5-O3	64.1									
Sb5-O11	31.7	16.6	14.1	14.5	80.4	33.0				
Sb5-O12	36.2	100.	99.4	99.8	96.7	93.4	98.4	99.9	99.6	99.0
Sb6-O2	17.1									
Sb6-O3	98.8	96.0	97.7	96.9	94.4	70.0	63.9	68.7	63.3	59.5
Sb6-O8	35.4	99.6	99.3	97.5	97.6	99.4	98.4	99.3	98.8	98.1
Sb7-O4		32.4	27.7	11.0	11.6					
Sb7-O8	92.1						83.2	90.4	84.3	86.9
Sb7-O9	30.8	100	100	100	100	100	100	100	100	100
Sb8-O1	99.2	100	100	100	100	96.7	99.2	100	99.9	99.5
Sb8-O11	14.3						81.8	90.5	91.8	94.3

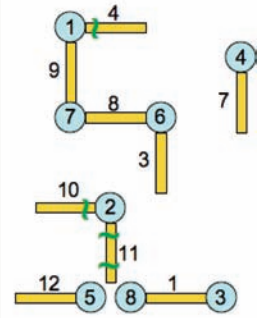

Figure 10. Percentage of Sb−O bonds formed between 0 and 1 ns. Each column is a successive 100 ps time block in the simulation.

	11	12	13	14	15	16	17	18	19	20
Sb1-O2	66.5	61.1	73.0	54.7	72.8	57.7	55.2	43.4	60.5	25.9
Sb1-O4	75.3	65.4	58.9	88.8	52.4	83.3	84.5	85.3	81.0	93.9
Sb1-O9	98.5	99.7	98.8	99.7	99.2	99.9	99.9	99.6	99.1	100
Sb2-O11	100	99.8	100	100	100	100	100	100	100	100
Sb3-O1	99.9	99.7	99.9	100	99.7	98.3	99.2	98.7	97.2	98.7
Sb3-O3	52.8	63.1	51.5		43.2	24.2	28.4	28.5	25.8	45.3
Sb4-O7	100	99.8	99.3	100	99.9	100	99.9	100	100	100
Sb5-O12	100	100	100	100	100	100	100	100	100	100
Sb6-O3	29.0	15.3	17.6	67.5	34.0	62.8	45.5	47.2	45.0	54.3
Sb6-O8	99.3	99.5	99.8	96.4	99.3	98.2	99.3	99.1	99.5	99.1
Sb7-O8	92.0	96.1	81.8	82.1	88.1			11.9	10.9	15.5
Sb7-O9	99.9	99.9	100	100	99.9	100	100	100	99.9	100
Sb7-O10									49.4	
Sb8-O1	98.5	99.6	99.2	99.5	98.3	100	100	100	100	100
Sb8-O11	98.2	99.0	94.7	99.1	98.7					

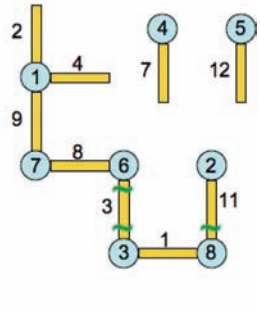

Figure 11. Percentage of Sb−O bonds formed between 1 and 2 ns. Each column is a successive 100 ps time block in the simulation.

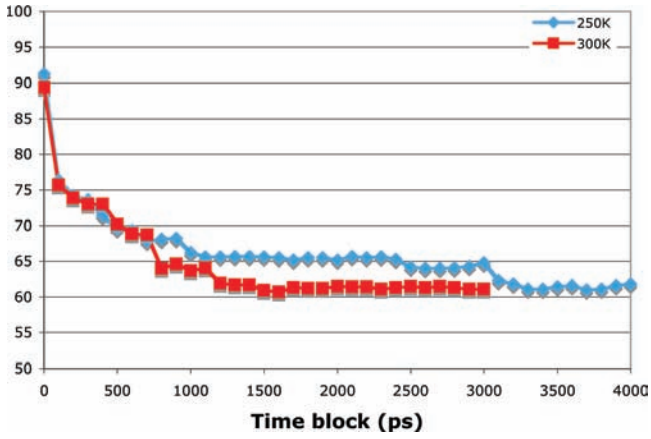

Figure 12. Percentage of Sb−O bonds starting from the crystal structure of 16 $SbCl_3$ and 24 dioxane in a 17 × 17 × 17 $Å^3$ simulation cell at 250 and 300 K.

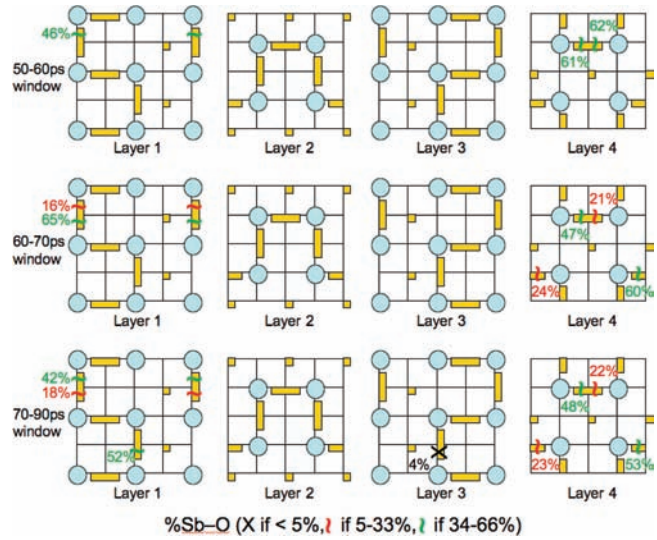

Figure 13. Sb−O bonds breaking in the initial heating and equilibration of the 16 $SbCl_3$ and 24 dioxane crystal structure.

The experimental melting temperature of the crystal is in the 420−430 K range. To observe what happens when the crystal is "melted", the 300 K structure was slowly heated (at a rate of 2.5 ps per 10 K increase) to 430 K and allowed to equilibrate over a 50 ps window. Data was then collected for 1 ns of dynamics. Over this range, %SbO falls slightly to 57% and stays constant. To reach a disordered liquid state, the structure was then heated from 430 to 560 K under the same conditions. During the 1 ns of dynamics at 560 K, %SbO drops further to 51%. Snapshots for the simulations at 430 and 560 K can be found in Supporting Information. We find that the number of labile bonds increases with higher temperatures where more than half the bonds are labile and the structure is disordered.

In contrast, at 250 K where only 17 of the 48 bonds are labile on average, a sufficient number of intact bonds continue to

TABLE 6: Solvation Energies in kcal/mol of $SbCl_3$ and Dioxane in Dielectrics Representing the Solution

		solvent		
		$\epsilon = 2.2$ ($SbCl_3$)	$\epsilon = 12.8$ (dioxane)	$\epsilon = 7.5$ (average)
solute	$SbCl_3$	−3.32	−8.29	−7.36
	dioxane	−3.06	−6.41	−5.81

enforce a relatively ordered structure. The $SbCl_3$ molecules in the crystal structure (see Figure 2) can be decomposed into two groups. Picture the 8 unique molecules in Layers 1 and 3 at corners of a cube, and the 8 molecules in Layers 2 and 4 at the corners of another cube. Thus, there are two chains of interconnected $SbCl_3$, each consisting of 8 $SbCl_3$ molecules. Although the crystal structure at 250 K has an equilibrium %SbO value of 61% (and not 100%), the 31 out of 48 intact Sb−O bonds has the same two groups of 8 $SbCl_3$ molecules each; that is, the crystal structure remains intact.

16 $SbCl_3$/24 Dioxane Random Starting Configuration. To generate random starting configurations that do not initially have bad van der Waals overlap, we randomly placed the molecules in a 25 × 25 × 25 Å^3 simulation cell, minimized the structure, then compressed the cell lengths to 17 × 17 × 17 Å^3 at 0.4 Å per picosecond. Figure 14 shows how the percentage of Sb−O bonds formed varies at 250 and 300 K. The average percentage of Sb−O bonds formed over the entire 4 ns simulation is 42.1% at 250 K and 41.3% at 300 K. These values are close to the 8 $SbCl_3$/12 dioxane system where approximately 45% of the Sb−O bonds are formed at the same density corresponding to the crystal structure. In Figure 15, we analyze four snapshots of the 300 K simulation. The bonds shown in each snapshot are averaged over 100 ps windows.

Early in the simulation (0.1−0.2 ns window), approximately half of the $SbCl_3$ molecules have two dioxanes attached for more than two-thirds of the simulation window (most of these are over 90%), while the other half have just one dioxane. Sb12 (top structure in first column of Figure 15) has a third dioxane (#8) bound for only 22% of the simulation. At the end of 1 ns (second column of Figure 15), we see several changes. Sb12 and Sb6 are no longer connected. Sb4 connects to Sb3 via dioxane 13, but loses its connection to Sb5. Meanwhile, the Sb10 and Sb13 structure has picked up Sb16 forming a larger structure. Up to this point, the range of structures we have observed are similar to those in the smaller 8 $SbCl_3$/12 dioxane system. At the end of 2 ns (third column of Figure 15), a relatively large structure is formed when Sb5 and Sb6 join the Sb10−Sb13−Sb16 substructure to create a network connecting 5 $SbCl_3$ molecules. Sb6 actually makes connections to four different dioxanes. Two of these interactions are stable. The third is more labile; it partially bonds to dioxane 14 (52%) and dioxane 10 (16%). This network is rather short-lived. At the end of 3 ns (fourth column of Figure 15), a stable network containing 4 $SbCl_3$ molecules is formed, consisting of Sb5, Sb10, Sb9, and Sb14.

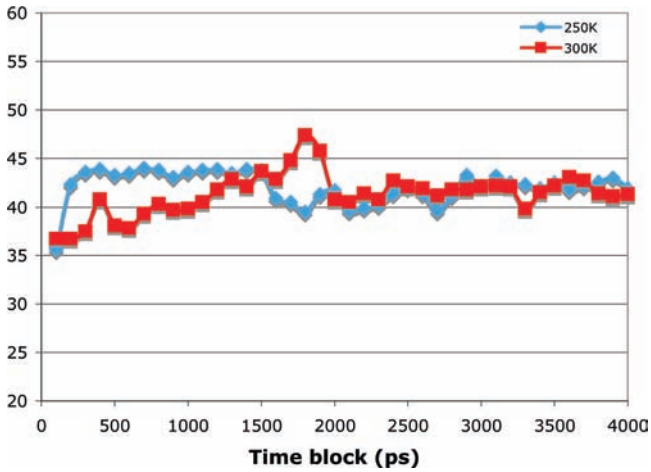

Figure 14. Percentage of Sb−O bonds formed starting from random configurations of 16 $SbCl_3$ and 24 dioxane in a 17 × 17 × 17 Å^3 simulation cell at 250 and 300 K.

Over the next 1 ns, while there are connections made and broken similar to those shown in Figure 15, there is no overall increase in the size of stable networks beyond 4 $SbCl_3$ molecules connected together. Also note that throughout the 4 ns simulation only 13−15 of the 16 $SbCl_3$ molecules have bonds to at least a single dioxane; that is, 1−3 remain unattached. Considering the dioxane molecules, only 15−16 out of 24 have at least one bond to a $SbCl_3$ molecule; that is, 8−9 remain unattached. In our analyses, we have not counted Sb−O bonds that are found less than 5% of the time in a 100 ps window. On average, 19−22 Sb−O bonds are made. This corresponds very closely to the 41% value of %SbO for this simulation.

In the previous section, we saw that the crystal structure, while showing some disorder, still maintains 61% of the Sb−O bonds. Thus, we can consider a random starting configuration to have reached the self-assembled crystal (dynamically disordered of course) if the percentage of Sb−O bonds formed reaches 61%. From Figure 14, we see that %SbO climbs quickly up to 41% and then holds steady. Therefore, there is an important transition on a much longer time scale that we have not captured with our 4 ns simulation. Given that crystallization in real time takes much longer than nanoseconds, simply running the simulation longer in the hope of seeing this transition is impractical. What important transitions are needed for the disordered structure at 41% to climb to 61% en route to forming the crystal? Our efforts to bridge this gap and explore what happens in between these two limiting values is described in the next section.

Bridging the Gap in the 16 $SbCl_3$/24 Dioxane System. On examining the crystal structure, we see an important repeating motif involving a network of 4 $SbCl_3$ molecules. Two examples are highlighted in Figure 16 for Layer 1 and Layer 2 of the crystal. Similar repeating motifs are found in Layer 3 and Layer 4. These motifs are also found crisscrossing in and out of the (layer) planes. There are 4 along the horizontal lines and 4 more along the vertical lines for a grand total of 12. If we represent this motif as a "square" for purposes of analysis as shown in Figure 16, then the unit cell of 16 $SbCl_3$ and 24 dioxanes consists of two interpenetrating "cubes"; each "cube" has six "square" faces, and each face represents one repeating motif. This gives a total of 12 "square" faces or 12 repeating motifs (which are open infinite chains) in the crystal structure. Our hypothesis was to examine if formation of this repeating motif would allow it to act as a template that would generate the ordered crystal structure.

In the previous section, we saw that one stable structure with 4 connected $SbCl_3$ molecules was formed involving Sb5, Sb10, Sb9 and Sb14. It is however missing the important connection between Sb5 back to Sb14 via dioxane 21 that would form the infinite repeating motif in the crystal. Starting with the structures represented by the rightmost column in Figure 15 (i.e., the 3 ns mark), we applied a force constant restraint of 100 kcal/Å^2 with an equilibrium Sb−O bond of 2.75 Å between dioxane 21 and Sb14 to form the new connection. To ensure that the rest of the

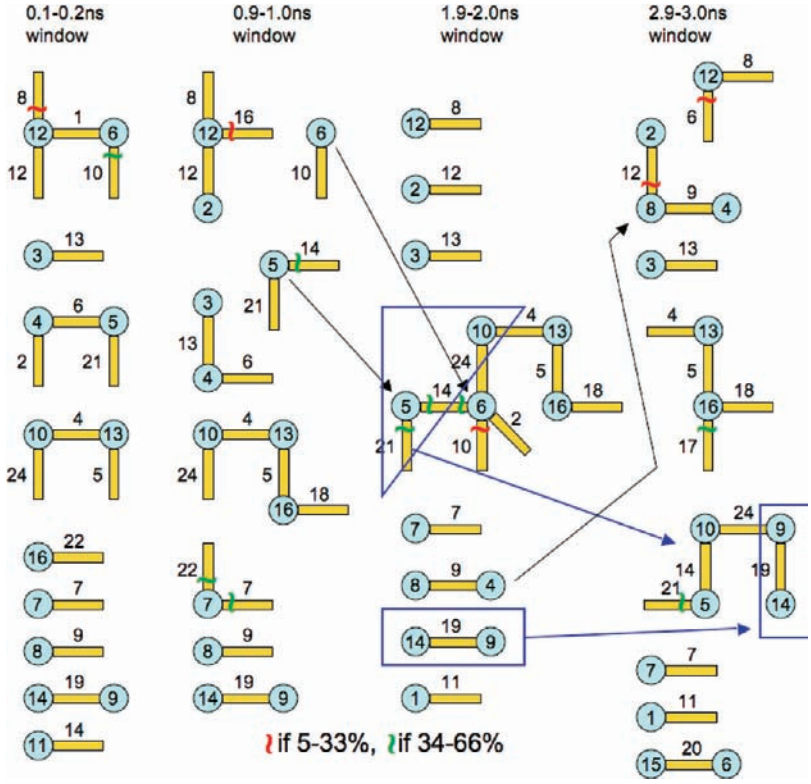

Figure 15. Snapshots of the 16 $SbCl_3$ and 24 dioxane simulation starting from a random configuration at 300 K.

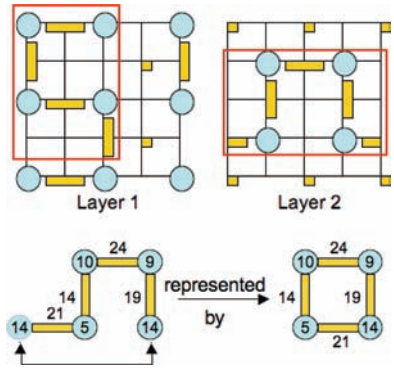

Figure 16. Repeating motif involving 4 $SbCl_3$ molecules.

network did not break up while connecting this last bond, similar restraints were placed on the other seven Sb−O bonds. Once the last bond was formed, we reduced all 8 constraints to 50 kcal/Å^2 and analyzed the molecular dynamics data over the next 2 ns. In our analysis, we will represent this structure as a square since Sb5 is connected to Sb14, albeit in an open infinite chain (see lower panel of Figure 16). Several snapshots are shown in Figure 17. Similar to those in Figure 15, the bonds shown in Figure 17 in each snapshot are averaged over 100 ps windows.

The leftmost column of Figure 17 is identical to the rightmost column in Figure 15. After the Sb5−Sb10−Sb-9−Sb14 repeating motif is formed, we see early in the simulation (0.0−0.1 ns window) that a second network of 4 $SbCl_3$ molecules consisting of Sb8, Sb4, Sb16, and Sb13 is formed, but this structure is short-lived. In the 0.7−0.8 ns window, a weak network consisting of 3 $SbCl_3$ molecules (Sb2, Sb8, Sb4) and 3 dioxanes (15, 12, 9) begins to persist although two of the bonds are very labile. Meanwhile, the original repeating motif has picked up two more dioxanes. Dioxane 2 is somewhat labile interacting with Sb5. Dioxane 3 on the other hand forms a stable interaction with Sb9. In the 0.9−1.0 ns window, dioxane 3 bridges the repeating motif with the weak Sb2−Sb8−Sb4 network. This interaction however is dissolved in the 1.2−1.3 ns window. However, we see that the bonds holding together the Sb2−Sb8−Sb4 network are becoming more stable. In the 1.7−1.8 ns window, dioxane 15 is still partially labile while dioxane 12 is stable connecting Sb2 and Sb8. Another smaller structure that grows in stability is the Sb13−Sb16 structure. While present in the first two columns, it disappears in the 0.7−0.8 ns window and reappears in the 0.9−1.0 ns window. In the 1.2−1.3 ns window, dioxanes 4, 5, and 18 remain intactly connected to Sb13 and Sb16.

Before the Sb5−Sb10−Sb-9−Sb14 motif was completed (by applying bond restraints to bridge Sb5 and Sb14 via dioxane 21), the %SbO was stable at 42%. After the motif is formed, this value increases to 50%. In the last column of Figure 17, 26 out of 48 Sb−O bonds are relatively intact. Compare this to an average of just 20 Sb−O bonds without the motif structure (Figure 15). Forming one bond (dioxane 21 to Sb 14) has promoted the formation of other Sb−O bonds in the system. We therefore suggest that the templating of this 4 $SbCl_3$ repeating motif is a key step en route to forming the fully ordered crystal. The %SbO value of 50% is also almost midway between the converged values of 42% starting from a random configuration and 61% starting from the crystal.

In the previous section, we observed that melting the crystal by heating to 560 K leads to a disordered state with a %SbO value of 51%, also midway between the 42% and the 61% gap. An analysis of this "liquid" structure shows similarities to the structures in Figure 17, albeit with more labile bonds because of the higher temperature (see Supporting Information for detailed analysis). This supports our suggestion that a key interaction bridging the disordered liquid state and the semiordered solid state is the formation of the 4 $SbCl_3$ open chain repeating motif.

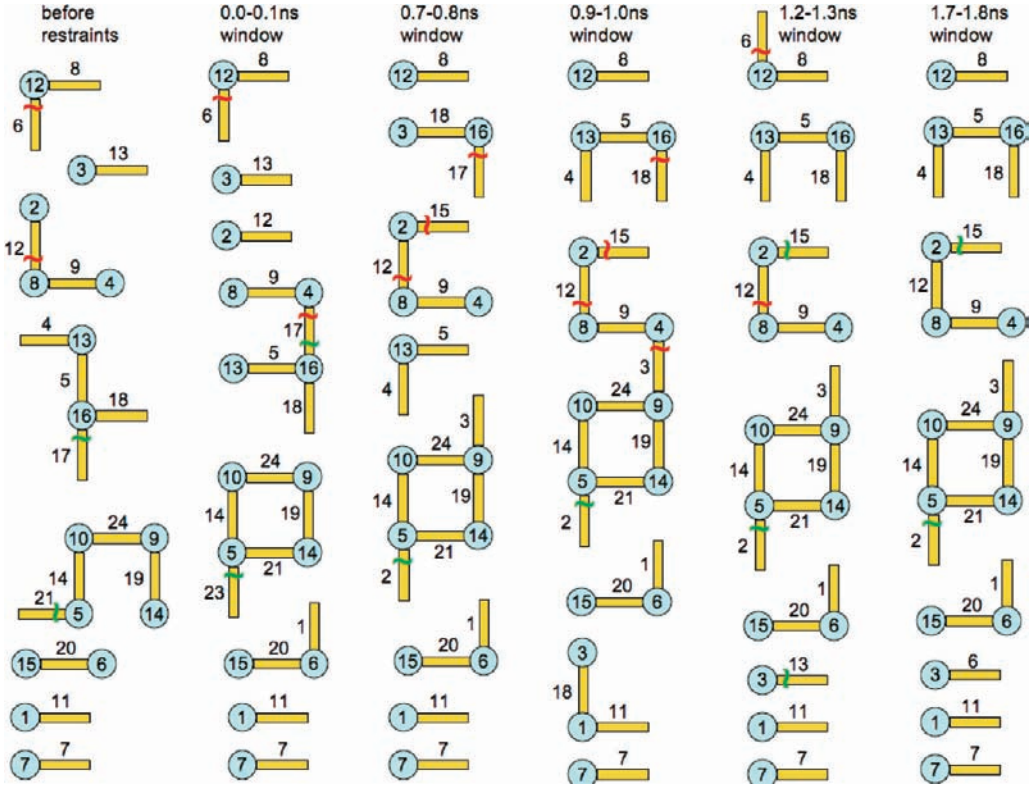

Figure 17. Snapshots of the 16 $SbCl_3$ and 24 dioxane simulation at 300 K with restraints on a four-$SbCl_3$ structural motif.

Conclusion

To study the self-assembly of a 2:3 ratio of $SbCl_3$ and 1,4-dioxane into a cubic structure, we parametrized the system and ran molecular dynamics simulations using ReaxFF. Since each $SbCl_3$ molecule can form three Sb−O bonds, a perfect cube can, in theory, be assembled with 8 $SbCl_3$ molecules in each corner bridged by 12 dioxane molecules. We found that this perfect cube is not stable in the 8 $SbCl_3$/12 dioxane system because there is too much void space in the center of a perfect cube and the Sb−O bonds, although directional, are very weak (∼7 kcal/mol each). The disordered structure at a density of 1.19 g/cm^3 has a %SbO value of 38% at 300 K. This value is very similar to 37% obtained when starting from a random configuration. If the system is compressed to the experimental density of 1.95 g/cm^3, the structure remains disordered although %SbO rises to 45%.

The crystal structure obtained from X-ray crystallography is an interpenetrating extended cubic structure with a 16 $SbCl_3$/24 dioxane unit cell. Because the Sb−O bonds are only marginally stronger than the dispersion forces of a corresponding liquid mixture, the dynamics of the crystal structure leads to a partially disordered structure with a %SbO value maintained at 61%. This structure is still sufficiently ordered with approximately three-quarters (31 out of 48) of Sb−O bonds intact although several of them show some labilily. Starting from a random configuration, the %SbO value only rises to a converged value of 41% suggesting that there is an important transition on a much longer time-scale that cannot be captured in a simulation of several nanoseconds. By adding a bond restraint to a four $SbCl_3$ substructure so that it forms a key repeating motif observed in the crystal structure, we found that additional Sb−O bond formation was promoted and %SbO rises to 50%. Similarly, when heating the crystal structure past its melting point to a disordered liquid, %SbO falls to the same value, and a similar range of substructures is observed.

We can therefore conclude that when $SbCl_3$ and 1,4-dioxane are mixed, they rapidly form 1:1 adducts, which then slowly grow so that substructures containing a network of two and three $SbCl_3$ molecules (with associated dioxanes) are formed. Once a stable network of four $SbCl_3$ molecules is formed, a slow transition that connects these units to form long open chains can act as a template to form additional Sb−O bonds. We find that the formation of one of these repeating motifs leads to a structure with a %SbO value midway between a disordered structure starting from a random configuration and a semiordered structure starting from the perfect crystal.

Acknowledgment. This research was supported by an American Chemical Society Petroleum Research Fund grant (PRF# 46700-GB10), an award from the Research Corporation, and a Camille and Henry Dreyfus Foundation Start-up Award.

Supporting Information Available: The four isomorphous dioxanate crystal structures of $AsCl_3$, $AsBr_3$, $SbCl_3$, $SbBr_3$ have been deposited at the Cambridge Crystallographic Data Centre and allocated the deposition numbers 735003 through 735006. Comparative discussion of our present X-ray structure with reference 15 is included. More detailed analyses of several simulations and accompanying figures are also discussed. The full training set and force field parameters can also be found in Supporting Information.This material is available free of charge via the Internet at http://pubs.acs.org.

References and Notes

(1) McCullagh, M.; Prytkova, T.; Tonzani, S.; Winter, N. D.; Schatz, G. C. *J. Phys. Chem. B* **2008**, *112*, 10388.
(2) Patil, A. J.; Mann, S. *J. Mater. Chem.* **2008**, *18*, 4605.
(3) Ofir, Y.; Samanta, B.; Rotello, V. M. *Chem. Soc. Rev.* **2008**, *37*, 1814.
(4) Morris, R. E.; Wheatley, P. S. *Angew. Chem., Int. Ed.* **2008**, *47*, 4966.

(5) Fujita, N.; Shinkai, S.; James, T. D. *Chem. Asian J.* **2008**, *3*, 1076.
(6) Ariga, K.; Hill, J. P.; Lee, M. V.; Vinu, A.; Charvet, R.; Acharya, S. *Sci. Technol. Adv. Mater.* **2008**, *9*, 96.
(7) Kelley, C. J. M., P. A. *J. Am. Chem. Soc.* **1943**, *65*, 1307.
(8) Doak, G. O. *J. Am. Pharm. Assoc.* **1934**, *23*, 541.
(9) McCusker, P. A. C., B. C. *J. Am. Chem. Soc.* **1942**, *64*, 614.
(10) Eveland, J. R.; Whitmire, K. H. *Inorg. Chim. Acta* **1996**, *249*, 41.
(11) Bowmaker, G. A.; Hannaway, F. M. M.; Junk, P. C.; Lee, A. M.; Skelton, B. W.; White, A. H. *Aust. J. Chem.* **1998**, *51*, 331.
(12) Genge, A. R. J.; Hill, N. J.; Levason, W.; Reid, G. *J. Chem. Soc., Dalton Trans.* **2001**, 1007.
(13) Barton, A. J.; Hill, N. J.; Levason, W.; Patel, B.; Reid, G. *Chem. Commun.* **2001**, 95.
(14) Barton, A. J.; Hill, N. J.; Levason, W.; Reid, G. *J. Chem. Soc., Dalton Trans.* **2001**, 1621.
(15) Zang, X. S.; Chen, Y. R.; Luan, S. R.; Zhong, G. Q.; Guo, Y. C. *Chin. J. Inorg. Chem.* **2001**, *17*, 901.
(16) Choi, H. J.; Suh, M. P. *J. Am. Chem. Soc.* **2004**, *126*, 15844.
(17) Fletcher, A. J.; Cussen, E. J.; Prior, T. J.; Rosseinsky, M. J.; Kepert, C. J.; Thomas, K. M. *J. Am. Chem. Soc.* **2001**, *123*, 10001.
(18) Hawxwell, S. M.; Espallargas, G. M.; Bradshaw, D.; Rosseinsky, M. J.; Prior, T. J.; Florence, A. J.; van de Streek, J.; Brammer, L. *Chem. Commun.* **2007**, 1532.
(19) Uemura, K.; Kitagawa, S.; Kondo, M.; Fukui, K.; Kitaura, R.; Chang, H. C.; Mizutani, T. *Chem.—Eur. J.* **2002**, *8*, 3586.
(20) van Duin, A. C. T.; Dasgupta, S.; Lorant, F.; Goddard, W. A. *J. Phys. Chem. A* **2001**, *105*, 9396.
(21) Strachan, A.; van Duin, A. C. T.; Chakraborty, D.; Dasgupta, S.; Goddard, W. A. *Phys. Rev. Lett.* **2003**, 91.
(22) Nielson, K. D.; van Duin, A. C. T.; Oxgaard, J.; Deng, W. Q.; Goddard, W. A. *J. Phys. Chem. A* **2005**, *109*, 493.
(23) Cheung, S.; Deng, W. Q.; van Duin, A. C. T.; Goddard, W. A. *J. Phys. Chem. A* **2005**, *109*, 851.
(24) Ludwig, J.; Vlachos, D. G.; van Duin, A. C. T.; Goddard, W. A. *J. Phys. Chem. B* **2006**, *110*, 4274.
(25) Chenoweth, K.; van Duin, A. C. T.; Persson, P.; Cheng, M. J.; Oxgaard, J.; Goddard, W. A. *J. Phys. Chem. C* **2008**, *112*, 14645.
(26) *Jaguar.* v6.0; Schrodinger, LLC: Portland, OR, 2005.
(27) Becke, A. D. *Phys. Rev. A* **1988**, *38*, 3098.
(28) Becke, A. D. *J. Chem. Phys.* **1993**, *98*, 5648.
(29) Lee, C.; Yang, W.; Parr, R. G. *Phys. Rev. B* **1988**, *37*, 785.
(30) Vosko, S. H.; Wilk, L.; Nusair, M. *Can. J. Phys.* **1980**, *58*, 1200.
(31) Hay, P. J.; Wadt, W. R. *J. Chem. Phys.* **1985**, *82*, 299.
(32) Chenoweth, K.; van Duin, A. C. T.; Goddard, W. A. *J. Phys. Chem. A* **2008**, *112*, 1040.
(33) Lindquist, I.; Niggli, A. *J. Inorg. Nucl. Chem.* **1956**, *2*, 345.
(34) Berendsen, H. J. C.; Postma, J. P. M.; van Gunsteren, W. F.; DiNola, A.; Haak, J. R. *J. Chem. Phys.* **1984**, *81*, 3684.
(35) *Spartan. '*06; Wavefunction, Inc.: Irvine, CA, 2006.
(36) Truskett, T. M.; Dill, K. A. *J. Chem. Phys.* **2002**, *117*, 5101.

JP908205X